Stellar mass fraction and quasar accretion disk size in SDSS J1004+4112 from photometric follow-up

R. Forés-Toribio[1,2], J. A. Muñoz[1,2], C. Fian[1], J. Jiménez-Vicente[3,4] and E. Mediavilla[5,6]

[1]Departamento de Astronomía y Astrofísica, Universidad de Valencia, E-46100 Burjassot, Valencia, Spain. email: raquel.fores@uv.es

[2]Observatorio Astronómico, Universidad de Valencia, E-46980 Paterna, Valencia, Spain

[3]Departamento de Física Teórica y del Cosmos, Universidad de Granada, Campus de Fuentenueva, 18071 Granada, Spain

[4]Instituto Carlos I de Física Teórica y Computacional, Universidad de Granada, 18071 Granada, Spain

[5]Instituto de Astrofísica de Canarias, Vía Láctea S/N, La Laguna, E-38200, Tenerife, Spain

[6]Departamento de Astrofísica, Universidad de la Laguna, La Laguna, E-38200, Tenerife, Spain

Abstract. The gravitational lens SDSS J1004+4112 was the first discovered system where a background quasar is lensed by a galaxy cluster instead of a single galaxy. We use the 14.5-year r-band light curves together with the recently measured time delay of the fourth brightest quasar image (Muñoz et al. (2022)) and the mass model from Forés-Toribio et al. (2022) to study the microlensing effect in this system. We constrain the quasar accretion disk size to $R_{1/2} = 5.3^{+1.3}_{-0.7}\sqrt{M/0.3M_\odot}$ light-days at 2407Å in the restframe which is compatible with most previous estimates. We also infer the fraction of mass in stars at the positions of the quasar images: $\alpha_A = 0.058^{+0.024}_{-0.032}$, $\alpha_B = 0.048^{+0.032}_{-0.014}$, $\alpha_C = 0.018^{+0.015}_{-0.018}$ and $\alpha_D = 0.008^{+0.033}_{-0.008}$. The stellar fraction estimates are reasonable for intracluster medium although the stellar fractions at images A and B are slightly larger, suggesting the presence of a near undetected galaxy.

Keywords. Gravitational lensing: micro, Galaxies: clusters: intracluster medium, Accretion, accretion disks, quasars: individual: SDSS J1004+4112

1. Introduction

The first example of a quasar lensed by a galaxy cluster was SDSS J1004+4112 (Inada et al. (2003)). Since the deflector mass is larger than for the typical scenario of lensed quasars, the multiple images are formed far ($\sim$15") from the brightest cluster galaxy. With this particular configuration, the light from the quasar images travels mainly through the intracluster medium and the impact of microlensing was expected to be small. However, soon after its discovery, microlensing variability was reported in the blue wing of the broad emission lines of image A (Richards et al. (2004); Gómez-Álvarez et al. (2006); Lamer et al. (2006); Motta et al. (2012); Fian et al. (2018); Popović et al. (2020); Fian et al. (2021)), as well as in the continuum emission of the accretion disk (Fohlmeister et al. (2008); Chen et al. (2012); Fian et al. (2016)).

From the microlensing variability in each different quasar image we can infer the accretion disk size of the quasar and the stellar mass fraction in the galaxy cluster where the

images are located. In order to do so, we use the light curves from Muñoz et al. (2022). These light curves were acquired at the Fred Lawrence Whipple Observatory (FLWO) 1.2 m during 14.5 years. Given the length of the light curves, the time delay of image D was determined for the first time and it is the longest delay ever measured for a lensed quasar. Also, the time delays between images A, B and C were constrained more precisely than in the previous work of Fohlmeister et al. (2008). These three independent time delays are crucial to properly extract the microlensing variability in the light curves.

The newly measured time delay can also be used to refine the galaxy cluster mass model as in Forés-Toribio et al. (2022). The mass model was built incorporating these new measurements of time delays along with previous observations reported in Oguri (2010) (the images positions and flux ratios, the positions, luminosities and ellipticities of the galaxy cluster members, and the velocity dispersion of the brightest cluster galaxy). This mass model was able to precisely constrain the inner slope of the generalised Navarro-Frenk-White profile that was used to model the Dark Matter Halo of the cluster. The inclusion of the time delay of image D was directly related to this determination because its value strongly depends on the inner slope of this component (Kawano & Oguri (2006); Oguri (2010)). Apart from this determination, the convergence and shear at the quasar positions were computed from this mass model and are used to model the microlensing variability.

2. Methods and results

In order to estimate the microlensing variability, we need to remove the intrinsic variability produced by the quasar itself and the magnification that the lensing cluster provides to each image. To do so, we first smooth the light curves with a window of ten days to reduce the noise and we subtract one light curve to another after shifting them by their corresponding time delays, with this procedure the intrinsic variability is removed. The light curves that are going to be subtracted are fit with 5th order splines to interpolate their magnitudes when differentiated. To correct for the macro-magnification, we also subtract their magnitudes in infrared from Ross et al. (2009) which are expected to be only affected by macro-magnification. In this way, we compute the six independent microlensing differences between the images, i.e., A−B, C−B, D−B, A−C, D−C and A−D which are depicted in Figure 1.

With these residuals we construct histograms of microlensing differences by Monte Carlo sampling to account for observational errors. The histograms from observational data are compared with model histograms which depend on the half-light radius of the source, $R_{1/2}$, and the stellar fractions at each quasar image position, $\alpha = \kappa_*/\kappa$. These histograms are obtained from magnification maps computed with the Fast Multipole Method - Inverse Polygon Mapping (FMM-IPM) developed by Jiménez-Vicente & Mediavilla (2022). The magnification maps dimensions are $60 \times 60\ R_E$ with the convergence and shear from the mass model of Forés-Toribio et al. (2022) and with variable fraction of mass in stars. These stars have a mass of $0.3 M_\odot$ and are distributed randomly. Lastly the maps are convolved with different source sizes modelled as Gaussians.

The probability that a given set of parameters reproduce the observed microlensing differences, H, is:

$$P(H|R_{1/2}, \alpha_A, \alpha_B, \alpha_C, \alpha_D) \propto e^{-\chi^2/2} \tag{1}$$

where

$$\chi^2 = \sum_\mu \sum_i \left(\frac{h_\mu(i) - \tilde{h}_\mu(i; R_{1/2}, \alpha_X, \alpha_R)}{\epsilon_\mu(i)} \right)^2 . \tag{2}$$
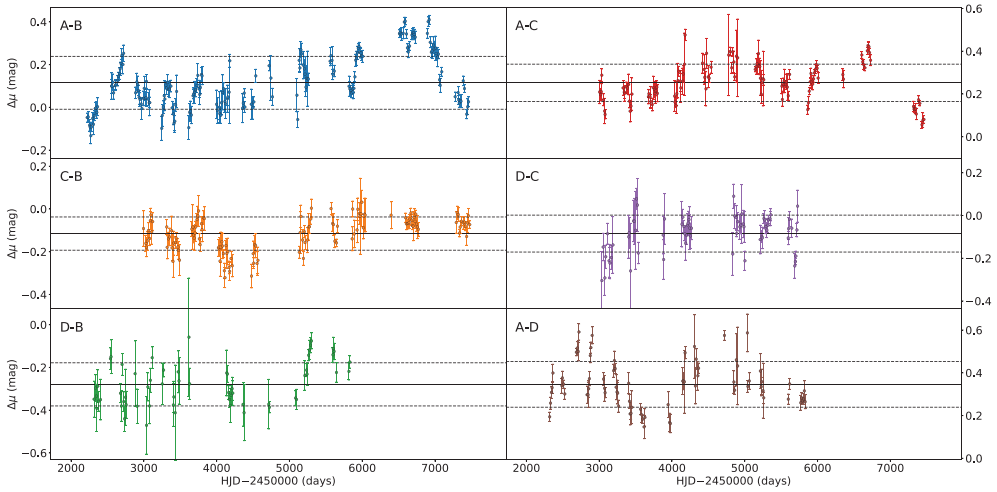
Figure 1. Microlensing differences between the four brightest quasar images. The solid black lines mark the average micro-magnification and the dashed lines show the standard deviation.

The first summation runs over the six microlensing differences and the second over the histogram bins. $h_\mu(i)$ is the ith bin of the normalised observed histogram, $\epsilon_\mu(i)$ is the error associated to that bin and $\tilde{h}_\mu(i; R_{1/2}, \alpha_X, \alpha_R)$ is ith bin of the difference of two model histograms for the given set of parameters (the half light radius of the source, $R_{1/2}$, the stellar fraction of the first image histogram, α_X, and the stellar fraction of the other image histogram, α_R).

We assign a logarithmic prior to the accretion disk half light radius and a uniform prior to the stellar fractions when their posterior probabilities are computed. We vary all the parameters but we keep the stellar fractions within a reasonable range according to the mass model of Forés-Toribio et al. (2022). With this procedure we can constrain the quasar accretion disk size to $R_{1/2} = 5.3^{+1.3}_{-0.7}\sqrt{M/0.3M_\odot}$ light-days at 2407Å in the restframe. However, the stellar fractions are mainly unconstrained as shown on the left panel of Figure 2.

Given that the source is properly constrained, we fix it to the central value and rerun the inference to attempt to determine confidence intervals for the stellar fractions. Under the hypothesis that the source size is $R_{1/2} = 5.3$ light-days, the probability distributions of the stellar fractions are presented in the right panel of Figure 2 and the central values and the 68% confidence intervals are $\alpha_A = 0.058^{+0.024}_{-0.032}$, $\alpha_B = 0.048^{+0.032}_{-0.014}$, $\alpha_C = 0.018^{+0.015}_{-0.018}$ and $\alpha_D = 0.008^{+0.033}_{-0.008}$.

3. Discussion and conclusions

In Figure 3 we compare previous size determinations at the same restframe wavelength and mean stellar mass with our inferred value. Our estimate is in tension with the determinations of Hutsemékers et al. (2023), Mosquera & Kochanek (2011) and Fohlmeister et al. (2008) who derived a smaller disk size. On the other hand, our value is compatible with the determinations of Fian et al. (2016), Jiménez-Vicente et al. (2014) and Motta et al. (2012). Given the length of the light curves, we achieve a tighter constraint on the source size than the majority of previous works.

Regarding the stellar fraction estimates, we can compare them with the stellar contributions from the brightest cluster galaxy (BCG) and the intracluster light (ICL) at the specific quasar positions derived from Kravtsov et al. (2018), DeMaio et al. (2018) and Henden et al. (2020) (see Table 1). According to these estimations, α_C and α_D lie

Table 1. Estimates of the stellar mass fraction from the brightest cluster galaxy and the intracluster light at the quasar image positions based on previous works.

BCG+ICL	K18	D18	H20
α_A	0.012 ± 0.007	0.006 ± 0.002	$0.012^{+0.022}_{-0.008}$
α_B	0.013 ± 0.008	0.007 ± 0.003	$0.013^{+0.025}_{-0.009}$
α_C	0.014 ± 0.009	0.008 ± 0.003	$0.011^{+0.022}_{-0.007}$
α_D	0.018 ± 0.010	0.038 ± 0.013	$0.022^{+0.028}_{-0.012}$

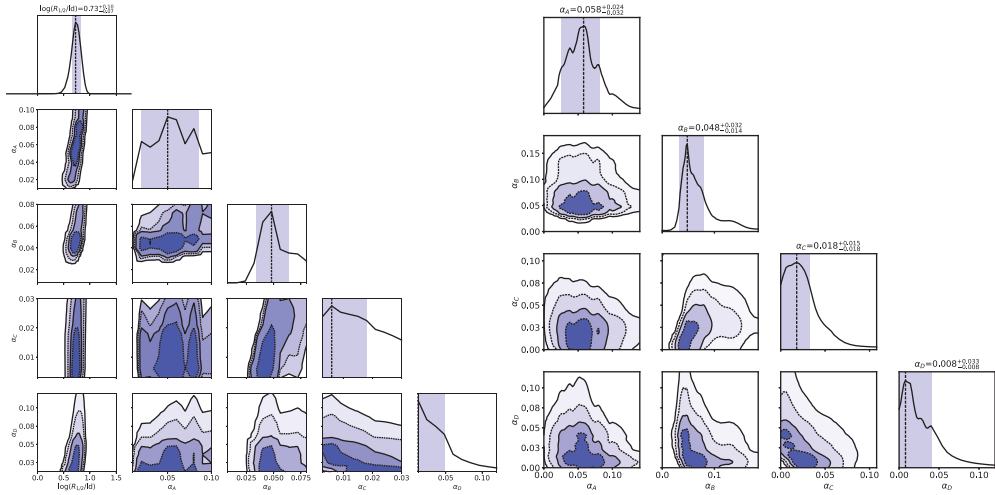K18 = Kravtsov et al. (2018), D18 = DeMaio et al. (2018) and H20 = Henden et al. (2020).

Figure 2. Probability distributions by pairs of parameters and marginalised distributions where the confidence intervals are reported at the 68% confidence level around the maximum. In the 2D plots, the 1-σ and 2-σ contours are marked with solid lines and the 0.5-σ and 1.5-σ are displayed as dashed lines. The left panel represents the joint inference for all five parameters ($R_{1/2}$, α_A, α_B, α_C and α_D) and the right panel shows only the inference for the stellar fractions when the source size is fixed to 5.3 light-days.
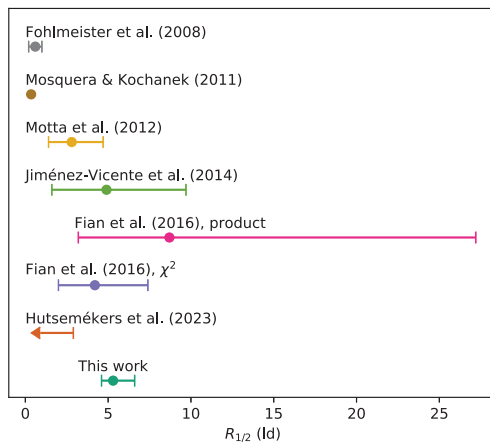

Figure 3. Quasar accretion disk size estimates for SDSS J1004+4112. The results are reported at $\lambda_{\rm rest}$=2407Å half-light radius in light-days for a mean stellar mass of $0.3M_\odot$.

around the expected values but at the image positions A and B we obtain slightly larger fractions. This may suggest the presence of undetected galaxy cluster members in those regions.

References

Chen, B., Dai, X., Kochanek, C. S., et al. 2012, *ApJ*, 755, 24.

DeMaio, T., Gonzalez, A. H., Zabludoff, A., et al. 2018, *MNRAS*, 474, 3009.

Fian, C., Guerras, E., Mediavilla, E., et al. 2018, *ApJ*, 859, 50.

Fian, C., Mediavilla, E., Hanslmeier, A., et al. 2016, *ApJ*, 830, 149.

Fian, C., Mediavilla, E., Motta, V., et al. 2021, *A&A*, 653, A109.

Fohlmeister, J., Kochanek, C. S., Falco, E. E., et al. 2008, *ApJ*, 676, 761.

Forés-Toribio, R., Muñoz, J. A., Kochanek, C. S., et al. 2022, *ApJ*, 937, 35.

Gómez-Álvarez, P., Mediavilla, E., Muñoz, J. A., et al. 2006, *ApJL*, 645, L5.

Henden, N. A., Puchwein, E., & Sijacki, D. 2020, *MNRAS*, 498, 2114.

Hutsemékers, D., Sluse, D., Savić, D., et al. 2023, *A&A*, 672, A45.

Inada, N., Oguri, M., Pindor, B., et al. 2003, *Nature*, 426, 810.

Jiménez-Vicente, J. & Mediavilla, E. 2022, *ApJ*, 941, 80.

Jiménez-Vicente, J., Mediavilla, E., Kochanek, C. S., et al. 2014, *ApJ*, 783, 47.

Kawano, Y. & Oguri, M. 2006, *PASJ*, 58, 271.

Kravtsov, A. V., Vikhlinin, A. A., & Meshcheryakov, A. V. 2018, *Astron. Lett.*, 44, 8.

Lamer, G., Schwope, A., Wisotzki, L., et al. 2006, *A&A*, 454, 493.

Mosquera, A. M. & Kochanek, C. S. 2011, *ApJ*, 738, 96.

Motta, V., Mediavilla, E., Falco, E., et al. 2012, *ApJ*, 755, 82.

Muñoz, J. A., Kochanek, C. S., Fohlmeister, J., et al. 2022, *ApJ*, 937, 34.

Oguri, M. 2010, *PASJ*, 62, 1017.

Popović, L. Č., Afanasiev, V. L., Moiseev, A., et al. 2020, *A&A*, 634, A27.

Richards, G. T., Keeton, C. R., Pindor, B., et al. 2004, *ApJ*, 610, 679.

Ross, N. R., Assef, R. J., Kochanek, C. S., et al. 2009, *ApJ*, 702, 472.